# Effects of H19/SAHH/DNMT1 on the Oxidative DNA Damage Related to Benzo[a]Pyrene Exposure

**Ye Fu**
Shanxi Medical University
**Xuejing Li**
Shanxi Medical University
**Baolong Pan**
Shanxi Medical University
**Yingying Niu**
Shanxi Medical University
**Bin Zhang**
Shanxi Medical University
**Xinyu Zhao**
Shanxi Medical University
**Jisheng Nie**
Shanxi Medical University
**Jing Yang** ( yang_jin@sxmu.edu.cn )
Shanxi Medical University https://orcid.org/0000-0003-1740-2180

**Research Article**

**Keywords:** Polycyclic aromatic hydrocarbons; long non-coding RNA H19; Oxidative DNA damage; 8-oxoguanine DNA glycosylase 1, S-adenosylhomocysteine hydrolase, DNA methyltransferases

**Posted Date:** December 15th, 2021

**DOI:** https://doi.org/10.21203/rs.3.rs-944681/v2

# Abstract

The mechanisms that long noncoding RNA (lncRNA) *H19* binding to S-adenosylhomocysteine hydrolase (SAHH) interacted with DNA methyltransferase 1 (DNMT1) and then regulated DNA damage caused by PAHs remain unclear. A total of 146 occupational workers in a Chinese coke-oven plant in 2014 were included in the final analyses. We used high performance liquid chromatography mass spectrometry (HPLC-MS) equipped to detect urine biomarkers of PAHs exposure, including 2-hydroxynaphthalene (2-NAP), 2-hydroxyfluorene (2-FLU), 9-hydroxyphenanthrene (9-PHE), 1-hydroxypyrene (1-OHP). The levels of SAM and SAH in plasma were detected by HPLC-ultraviolet. By constructing various BEAS-2B cell models exposed to 16 μM Benzo[*a*]pyrene (BaP) for 24 h, toxicological parameters reflecting distinct mechanisms were evaluated. We documented that urinary 1-hydroxypyrene (1-OHP) levels were positively associated with blood *H19* RNA expression (*OR*: 1.51, 95% *CI*: 1.03 - 2.19), but opposite to plasma SAHH activity (*OR*: 0.63, 95% *CI*: 0.41 - 0.98) in coke oven workers. Moreover, by constructing various BEAS-2B cell models exposed to Benzo[*a*]pyrene (BaP), we investigated that *H19* binding to SAHH exaggerated DNMT1 expressions and activity. Suppression of *H19* enhanced the interaction of SAHH and DNMT1 in BaP-treated cells, decreased *OGG1* methylation, reduced oxidative DNA damage and lessened S phase arrest. However, *SAHH* or *DNMT1* single knockdown and *SAHH*/*DNMT1* double knockdown showed the opposite trend. A *H19*/SAHH/DNMT1 axis was involved in *OGG1* methylation, oxidative DNA damage and cell cycle arrest by carcinogen BaP.


# Background

Long noncoding RNAs (lncRNAs), a group of transcription of RNA from non-protein coding regions of the genome, are defined as endogenous cellular RNAs of longer than 200 nucleotides. They are implicated in a number of molecular functions, such as regulators of protein activity, molecular scaffolds, regulation of cell cycle and controllers of chromatin remodelling (Chen, 2016). *H19*, a multifunctional lncRNA, interacts with other proteins to exert functions as a ribonucleoprotein in tumorigenesis (Wang et al., 2019). Similar to Zhou J *et al.*(Zhou et al., 2015), a previous research by our team has revealed that *H19* binds to S-adenosylhomocysteine hydrolase (SAHH) and inhibits SAHH function, thus blocking *LINE-1* methylation in vitro (Fu et al., 2018). SAHH has been reported as a highly conserved enzyme capable of reversibly hydrolysing S-adenosylhomocysteine (SAH) and participates in S-adenosylmethionine (SAM)-dependent transmethylation reactions (Oksana et al., 2013). Gene methylation (5-methyl-cytosine), accomplished by the joint action of three SAM-dependent DNA methyltransferases (DNMT1, DNMT3A and DNMT3B), plays a critical role in mammalian development and physiology (Oksana et al., 2004). However, very little is known which type of DNA methyltransferase (DNMT1, DNMT3A or DNMT3B) would play a prominent role in the mechanism of *H19* binding to SAHH involved in gene methylation.

The genotoxic potency of PAHs is driven by excessive reactive oxygen species (ROS) production generated in the redox-cycling processes of their metabolic activation which overwhelms their elimination, and thus causing oxidative DNA lesion (Idowu et al., 2019). Base excision repair (BER) is responsible for repairing oxidative lesion (Whitaker et al., 2017). Eight-oxoguanine DNA glycosylase 1

(OGG1) acts as the key enzyme participated in the first step of the BER pathway (Gonçalves et al., 2017). Gene methylation, the important form of epigenetic modification in eukaryote genome, is known to regulate DNA damages caused by PAHs (Kanduri, 2015). Increased methylation of *OGG1* leads to the accumulation of DNA damage and further mutations (Alvarado-Cruz et al., 2017). Although the aspects of genetic alterations in population exposed to PAHs are well-documented (Moorthy et al., 2015), abnormal epigenetic regulation is still poorly understood.

Therefore, in order to explore effects of PAHs exposure on peripheral blood *H19* RNA expressions and plasma SAHH activity, we performed a cross-sectional observational study among occupational workers. Moreover, Benzo[*a*]pyrene (BaP), a potent carcinogen of PAHs, can cause a wide range of cell cycle perturbations, including S-phase accumulation, diminished capacity for DNA replication, and inhibition of cell proliferation. We hypothesized that *H19*/SAHH/DNMTs involved in *OGG1* methylation, oxidative DNA damage and cell cycle arrest in human after BaP exposure. To address our objectives, we used human lung epithelial cell lines treated with BaP as a model, and expected to illuminate the molecular mechanism of *H19*/SAHH/DNMTs regulating *OGG1* methylation, oxidative DNA damage and cell cycle arrest by carcinogen BaP.

## Methods

# Participants

A total of 146 occupational workers, who had worked for at least one year in a coke-oven plant in Taiyuan (Shanxi, China), were enrolled in the final analyses. And the workers who had worked on top-, side- and bottom-oven in the coke oven plant were mainly young and middle-aged (Youth age defined by WHO-2017: 15 - 44 years old). Exclusion criteria included pulmonary diseases, syphilis, cancer, kidney diseases and other factors which may interfere with research. And the participants were not exposed to known occupational carcinogens or dust during the past three months. Our research was approved by the Ethical Review Board of the School of Public Health, Shanxi Medical University, Shanxi, People's Republic of China. Peripheral blood (5 mL) and morning first urine (20 mL) samples from all study population were collected in the morning of the same day. Plasma, which would be used to test the levels of SAM and SAH, was separated within 4 h after collection and then stored at -80°C.

# Determination of PAHs metabolites

The detection of the concentrations of four PAHs metabolites in urine by High performance liquid chromatography (HPLC, Shimadzu Corp, JPN), including 2-hydroxynaphthalene (2-NAP),1-hydroxypyrene (1-OHP), 9-hydroxyphenanthrene (9-PHE) and 2-hydroxyfluorene (2-FLU), has been described in detail in previous studies (Yang et al., 2017). The quality control data were detailed in Table S1.

# Plasma SAHH activity

After pre-treated by 240 uL Trichloroacetic Acid (400 g/L) with an ice bath for 30 min, 1.2 mL plasma was centrifuged at 14000rpm at 4°C for 20 min, and then supernatant was separated and filtered. HPLC-

ultraviolet detection was used to measure plasma SAM and SAH concentrations according to a method presented elsewhere (Illamola et al., 2019). We quantified plasma SAM and SAH concentrations in accordance with the peak area with standard solutions of (0, 0.05078, 0.10156, 0.20312, 0.40625, 0.81250, 1.62500 and 3.25000 mg/L for SAM) and (0, 0.03125, 0.06250, 0.12500, 0.25000, 0.50000 and 1.00000 mg/L for SAH) to establish the retention time. The quality control data were detailed in Table S1.

# Cell culture

BEAS-2B, a human lung epithelial cell lines, were cultured under 5% $CO_2$ at 37°C in α-MEM growth medium (GE), supplemented with 100 mg/mL streptomycin, 100 U/mL penicillin and 10% fetal bovine serum (Gibco, Paisley, UK).

# Cell transfections

The inhibitions of *H19*, *SAHH* and *DNMT1* were obtained by siRNA (RiboBio, Guangdong, China) to construct the low-expression cell model. The oligo sequences were shown as below: 5'-CCCACAACAUGAAAGAAAUdTdT-3' and 5'-dTdTGGGUGUU-GUACUUUCUUUA-3' for *H19*, 5'-CAAGCTAACTGAGAAGCAAdTdT-3' and 5'-dTdTGUUCGAUUGACUCUUCGUU-3' for *SAHH*, 5'-GAAGAGACGTAGAGTTACAdTdT-3' and 5'-dTdTCUUCUCUGCAUCUCAAUGU-3' for *DNMT1*. WT-SAHH (1 - 432 aa), M1-SAHH (1 - 150 aa), M2-SAHH (151 - 300 aa), M3-SAHH (300 - 432 aa) mutant versions of SAHH were inserted into pCMV-GV141 vector (Genechem, Shanghai, China). For the transfection of siRNA or pCMV-GV141 vector, cells were transfected by Lipofectamine-RNAi MAX or Lipofectamine 2000 (Invitrogen, Carlsbad, CA, USA) following the manufacturer's instructions. After transfection, RNA or protein was extracted for analysis (Fig. S1A-1E).

# Cells treatments

Eight type cells (WT, si-*H19*, si-*SAHH*, si-*DNMT1*, si-*H19* + si-*SAHH*, si-*H19* + si-*DNMT1*, si-*SAHH* + si-*DNMT1*, and si-NC) were treated with BaP (Sigma-Aldrich, USA) at a single dose of 16 μM for 24 h to reflect distinct mechanisms. The dose and time in this study were selected based on our preliminary experiments, which suggested that cell viability decrease less than 15% (Yang et al., 2009).

# RNA extraction and Real-time quantitative reverse transcription PCR (RT-PCR)

TRIzon Reagent (CWbiotech, Beijing, China) was used to isolate total RNA from participants' peripheral blood or cell lines and then cDNA was synthesized by the use of Prime Script RT Master Mix (Takara, Dalian, China) according to the method described in previous researches (Fu et al., 2018). Quantitative RT-PCR was also performed as described previously. Table S2 lists the RT-PCR primers. The primers for *β-actin*, *H19*, *SAHH*, *GAPDH* and *DNMT1* were used as previously reported (Fu et al., 2018). The primer for *OGG1* was obtained from QuantiTect Primer Assays.

# Proteins extraction and Western Blot

The extractions of proteins were obtained by the same method as the previous research from cells (Fu et al., 2018). Equal amounts of protein were fractionated by different concentrations (7% and 10%) sodium dodecyl sulphate-polyacrylamide gel electrophoresis and subsequently transferred onto PVDF membranes (Millipore, MA, USA). The membranes were blocked in 5% skim milk with gentle rotation and then incubated overnight at 4°C with the indicated primary antibodies (DNMT1, 1:2000, GeneTex, USA; SAHH, 1:1000, Proteintech, IL, USA; DNMT3A, 1:4000, Proteintech; DNMT3B, 1:500, GeneTex; GAPDH or β-tubulin, 1:4000, CWbiotech). After additional incubation with anti-immunoglobin horseradish peroxidase-linked Ab (1:4000, CWbiotech) for 2 h at 37°C, the levels of immune complexes were visualized and quantified by scanning laser densitometry (Universal Hood □, Bio-Rad).

# RNA immunoprecipitation (RIP) analysis

RNA immunoprecipitation (RIP) experiments were performed as described previously (Fu et al., 2018). Reverse transcription was in a 30 mL reaction, followed by RT-PCR (see Table S2 for primer sequences).

# DNMT1 activity assay

The DNMT1 activity of cells was quantitated following the manufacturer's protocol (EpiQuik™ DNA Methyltransferase Activity/Inhibition Assay Kit, Epigentek, Germany), and was determined by monitoring the fluorescence product at 450 nm using SpectraMax M2.

# Co-immunoprecipitation (Co-IP) analysis

The extractions of proteins were obtained from cells using the same method as the previous research from cells (Fu et al., 2018). For vitro binding assay, identical amounts of SAHH in extractions of cells and equal volume of Mouse anti-DNMT1 antibody (GeneTex) were added in 1.5 mL tubes and rotated overnight at 4°C. Then 40 μL protein A/G beads (CWbiotech) were added and incubated with rocking for 4 h at 4°C. Protein A/G beads and protein bound to the beads were washed three times with 1 mL of ice-cold PBS to reduce the non-specific binding to the beads. Finally, the proteins bound to beads were analysed by western blot, and probed for SAHH using Rabbit anti-SAHH antibody.

# Immunofluorescence analysis

*H19* FISH experiments were carried out using Fluorescent In Situ Hybridization Kit (RiboBio) according to the manufacturer's instructions. The system used *H19*-Cy3 FISH Probe Mix (1:40, RiboBio) to treat cells overnight at 37°C, avoiding light. After hybridisation, cells were washed twice with hybrid cleaning solution □/□/□ (SSC with different concentrations) each for 5 min at 42°C, avoiding light. Following incubating with primary antibodies Rabbit anti-SAHH antibody (1:200, Proteintech) and Mouse anti-DNMT1 antibody (1:200, GeneTex) and fluorescent-labelled secondary antibodies (anti-mouse IgG coupled with Alexa Fluor 488 (1:200, Invitrogen), anti-rabbit IgG coupled with Alexa-Fluor-647 (1:400, Abcam, Cambridge, UK)). To stain the nuclei, cells were counterstained with 4, 6-diamidino-2-phenylindole (DAPI, 1:1000, Solarbio, USA) at room temperature for 10 min, avoiding light. Images were captured using a confocal microscope (FluoView FV10i, Olympus, Japan).

# DNA extraction and Gene methylation analysis

Genomic DNA extraction from cultured cells was performed using a Universal Genomic DNA Kit (CWbiotech) following the manufacturer's instructions. Genomic DNA (500 ng) was subsequently treated with sodium bisulfite by EZ DNA Methylation-Gold Kit (Zymo Research, USA) and amplified by PCR following the manufacturer's instructions. These PCR amplifications were isolated using the Pyrosequencing Work Station and sequenced by Pyromark Q96 MD pyrosequencing instrument (Qiagen, Germany) per the manufacturer's instructions. The dispensation order is 5'-ATCGAGATGGCTGATCGATGTCGGTTGATGTATCGT-3', and the analytic sequence of *OGG1*is 5'-YGGAGAATTGGGGTAYGAAGYGGGGTTTTGATGATTYGTA-3'. We detected DNA methylation levels at four CpG loci of *OGG1* in the first exon (Fig. 4A, left top).

# Oxidative DNA damage assessment

Total genomic DNA was extracted from cells as described previously. DNA was hydrolysed with nuclease P1 in a water bath at 37°C for 20 min, and then regulated pH to 7.5 - 8.5 by 1 M Tris. Hydrolytic DNA was incubated with alkaline phosphatase (1 unit / 100 μg DNA) at 37°C for 30 min, and then boiled for 10 min. The content of 8-OHdG was measured following the manufacturer's protocol (8-OHdG ELISA Kit, Abcam), and then the absorbance of samples was detected at 450 nm using SpectraMax M2.

# Cell cycle analysis

Cells were collected into 1.5 mL centrifuge tubes for flow cytometry by propidium iodide (PI) staining using DNA Content Quantitation Assay (Cell Cycle) (Solarbio) per the manufacturer's instructions. Flow cytometry was carried out by the same method as the previous research (Andres et al., 1998).

# Statistical analysis

Statistical representation of data was done by Statistical Package for Social Sciences version 22.0 (IBM SPSS, Chicago, IL, USA) software and SAS software version 9.4 (SAS Institute Inc., Cary, NC, USA).

Continuous data in vitro experiments were summarized as mean ± SD of at least three replicates and compared among means using ANOVA. Post hoc Dunnett analyses were used to analyse the differences between groups when the *P* value of the ANOVA was < 0.05. Covariance analysis was used to clarify whether there were differences among different types cells independent of exposure. *P* values < 0.05 were deemed to be statistically significant.

We substituted the concentrations below the LOD with 50% LOD, including four urinary PAHs metabolites, SAM and SAH. Continuous data in the cross-sectional study were expressed as medians (Med) and interquartile ranges (IQR), and compared with Kruskal-Wallis H test. Categorical data in the cross-sectional study were expressed as *N* (%) and compared with Chi-square test. To investigate the correlations and estimate the potential dose-repose relationship, we used logistic regression models adjusted confounders and restricted cubic spline model, respectively. By assigning the median value in quartiles as a continuous variable, the linear trend across 1-OHP concentration increasing with the

quartile can be estimated. The cut points for peripheral blood *H19* RNA expressions and plasma SAHH activity were defined as 14.42 and 0.83 in the present study, which were equivalent to the median.

## Results

# Effects of PAHs exposure on peripheral blood *H19* RNA expressions and plasma SAHH activity among 146 occupational workers

Table 1 summarizes the basic characteristics of study population based on the quartiles of urinary 1-OHP concentrations. There were no significant differences in age, smoking status, drinking status, heating mode, education ($P > 0.05$), even so, the marginal significances were showed in employment time ($P = 0.053$). The results indicated that with the rise of urinary 1-OHP levels, the concentrations of urinary 2-NAP, 2-FLU, 9-PHE and ΣOH-PAHs metabolites were also significantly elevated ($P < 0.001$). In addition, the detailed distributions of peripheral blood *H19* RNA expressions and plasma SAHH activity were given in Figure 1A with violin plots. An elevated median of peripheral blood *H19* RNA expressions was showed coupled with the increased quartile of urinary 1-OHP levels ($P = 0.479$), whereas the median of plasma SAHH activity was slightly reduced ($P = 0.844$). These findings are consistent with our previous experiments in human lung-derived cells treated with BaP (Fu et al., 2018).

The results of collinearity diagnostics showed that there was no collinearity between the four urinary PAHs metabolites, and also indicated that age was not collinear with employment time (Table S3). Figure 1C represented that peripheral blood *H19* RNA expressions were significantly increased when 1-OHP levels were lower than 0.09 μg/mM creatinine, and then maintained on the plateau phase while there is a marginal positive linear association between urinary 1-OHP levels and peripheral blood *H19* RNA expressions ($4^{th}$ vs. $1^{st}$ quartile = 3.44, 95% *CI*: 1.04 - 11.44, $P_{trend}$ =0.058) (Figure 1B). Nevertheless, the plasma SAHH activity was significantly reduced when 1-OHP levels were lower than 0.06 μg/mM creatinine (Figure 1C), showing a non-linear association between plasma SAHH activity and urinary 1-OHP concentrations ($P_{overall}$ = 0.089, $P_{non\text{-}linearity}$ = 0.030) (Figure 1C). However, the results did not reveal that 2-NAP, 9-PHE, 2-FLU and ΣOH-PAHs metabolites have significant effects on the expression of *H19* RNA in peripheral blood and plasma SAHH activity ($P > 0.05$, Table S4).

# *H19* interacts with SAHH at specific sites and then regulates DNMT1 in BEAS-2B cells exposed to BaP

Previous results have established that *H19* interacts with and suppresses SAHH expressions and activity would be enhanced by BaP (Fu et al., 2018), we performed RIP experiments using four types *SAHH*-overexpressing (WT-SAHH, M1-SAHH, M2-SAHH and M3-SAHH) cells to illuminate the binding sites between SAHH and *H19*. Whether exposed BaP or not, we observed an accessorial enrichment of *H19* in

SAHH-containing complexes in WT-SAHH, M1-SAHH and M2-SAHH cells (Fig. 2A), whereas M3-SAHH cells did not detectably elevate (Fig. 2A, left column 5 & right column 5). After BaP exposure, *H19* RNA expressions were inhibited in *SAHH*-overexpressing cells compare to WT cells (Fig. 2B, right column 3 - 6), particularly in M3-SAHH cells (Fig. 2B, right column 5). These results reveal that *H19* may bind to the 1 - 300 amino acid chain instead of 300-432 amino acid chain of SAHH.

To better understand which DNMTs is most affected by *H19* and SAHH, five types (WT, si-NC, si-*H19*, si-*SAHH*, si-*H19* + si-*SAHH*) cells were used to the further experiments (Fig. 2C & 2D). The exaggerated expression (Fig. 2C, right column) and activity (Fig.2D, right) of DNMT1 were observed in WT cells exposed to BaP, whereas a significant decrease in si-*H19*, si-*SAHH* and si-*H19* + si-*SAHH* cells exposed to BaP was observed (Fig. 2C, Fig. 2D). Collectively, these results revealed that *H19* binding to SAHH was more likely affected DNMT1 expressions and activity after BaP treatment.

# *H19* binding to SAHH interacts with DNMT1 in BEAS-2B cells exposed to BaP

As *H19* interacts with SAHH and shows characteristics of a ribonucleoprotein particle (Fu et al., 2018), we reasoned that *H19* binding to SAHH interacts with DNMT1 in BEAS-2B cells treated with BaP. In support of the assumption, we accessed Co-IP experiments to examine whether anti-DNMT1 antibody would be able to immunoprecipitate SAHH from complex. As shown in Fig. 3A, Co-IP analysis showed that a nearly 0.5-fold enrichment of SAHH in the DNMT1 antibody complex compared with WT cells. In addition, compared with the WT and si-NC cells, SAHH protein expression in si-*H19* cells was significantly increased after BaP exposure (Fig.3A, right column 3). However, the enrichment of SAHH in DNMT1-containing complex between WT and si-NC cells was similar (Fig.3A, left column 2 & right column 2).

Additionally, co-localization between endogenous *H19*, SAHH and DNMT1 was evaluated by confocal microscopy, predominantly in nucleus and perinuclear cytoplasm (Fig. 3B, white arrow). We found that the fluorescence intensity of DNMT1 was increased after BaP exposure for 24 hours (Fig.3B, column 4). The intracellular co-localization of *H19* and SAHH was consistent with the previous results (Fig. 3B, column 5). The increased fluorescence of purple intensity, which displayed the intracellular co-localization of *H19* and DNMT1, indicated a stronger steric interaction after BaP exposure for 24 hours, while fluorescence intensity was decreased in si-*H19* cells (Fig. 3B, column 6). In addition, the increased fluorescence intensity of SAHH and DNMT1 indicated a stronger steric interaction after BaP exposure for 24 hours and transfected with si-*H19* (Fig. 3B, column 7). Moreover, we also observed the increased fluorescence of blue violet, which displayed the intracellular co-localization of *H19*, SAHH and DNMT1, indicated a stronger steric interaction after BaP exposure for 24 hours (Fig. 3B, column 8). Together, these results suggest that *H19* binding to SAHH interacts with DNMT1 in BEAS-2B cells treated with BaP.

### *H19*/SAHH/DNMT1 regulates *OGG1* methylation

In order to test that *H19* binding to SAHH might interfere with DNMT1 and then regulate gene methylation in BaP-treated cells, we used eight type cells (WT, si-*H19*, si-*SAHH*, si-*DNMT1*, si-*H19* + si-*SAHH*, si-*H19* + si-*DNMT1*, si-*SAHH* + si-*DNMT1*, and si-NC) for BaP treatment. Pearson's correlation tests between methylation values (% 5-mC) each CpG locus in the first exon of *OGG1* and mean methylation value of four loci reveal high correlations (Pearson's *r* ranged from 0.63 to 0.86) (Fig. 4A). Results indicated that after BaP exposure, the levels of *OGG1* methylation in BEAS-2B cells increased significantly (Fig. 4B), whereas that in si-*H19* cells decreased (Fig. 4B, right column 3). Conversely, *SAHH* or *DNMT1* single knockdown exacerbated *OGG1* methylation (Fig. 4B, right column 4 & 5) and *SAHH*/*DNMT* double knockdown markedly aggravated the alteration (Fig. 4B, right column 8). Interestingly, although *H19* single knockdown obviously reduced *OGG1* methylation, *H19*/*SAHH* and *H19*/*DNMT1* double knockdown abolished this effect (Fig. 4B, right column 6). However, similar changes in *OGG1* methylation were observed in WT and si-NC cells (Fig. 4B, right column 2). Collectively, we concluded that *H19*/SAHH/DNMT1 regulates *OGG1* methylation in BEAS-2B cells treated with BaP.

## *H19*/SAHH/DNMT1 affects oxidative DNA damage and cell cycle arrest

Given the previous study conducted by our team indicating that *OGG1* methylation mediated oxidative DNA damage and cell cycle arrest associated with urinary 1-OHP concentrations in coke oven workers (Fu et al., 2019), we took an in vitro approach to examine whether *H19*/SAHH/DNMT1would regulate oxidative DNA damage and cell cycle arrest in accordance with the alteration of *OGG1* methylation for BaP exposure. Figure 4C & 4D exhibited the effects *H19*/SAHH/DNMT1 on the oxidative DNA damage and cell cycle arrest. After transfection, there was no significant change in the levels of 8-OHdG compared with WT cells (Fig. 4C, left column). However, the 8-OHdG levels were significantly increased in cells treated with BaP (Fig. 4C, right column). After BaP exposure, *H19* single knockdown slightly reduced 8-OHdG levels (Fig. 4C, right column 3), whereas *SAHH* or *DNMT1* single knockdown significantly elevated 8-OHdG levels (Fig. 4C, right column 4 & 5). After BaP treatment, *SAHH*/*DNMT1* double knockdown further dramatically increased 8-OHdG levels (Fig. 4C, right column 8), whereas *H19*/*SAHH* and *H19*/*DNMT1* double knockdown abrogated this effect (Fig. 4C, right column 6 & 7). Furthermore, the results of S phase arrest were parallel to 8-OHdG levels (Fig. 4D). Combined with our previous findings (Fu et al., 2019) and in vitro data (Fig. 4B), these results strongly support that *H19*/SAHH/DNMT1would regulate oxidative DNA damage and cell cycle arrest in BEAS-2B cells treated with BaP in keeping with *OGG1* methylation alterations.

## Discussion

In this cross-sectional study, we found that urinary 1-OHP levels were positively associated with peripheral blood *H19* RNA expression in occupational workers, while urinary 1-OHP levels were negatively associated with plasma SAHH activity. Using human lung epithelial cell lines (BEAS-2B) with BaP treatment as a model, we observed that *H19* binding to SAHH exaggerate DNMT1 expressions and

activity with BaP treatment. Suppression of *H19* enhanced the interaction of SAHH and DNMT1 induced by BaP. And *H19*/SAHH/DNMT1 may regulate *OGG1* methylation, oxidative DNA damage and S phase arrest in BEAS-2B cells exposed to BaP. As far as we know, this represents the first case that a *H19*/SAHH/DNMT1 axis involving in *OGG1* methylation, oxidative DNA damage and cell cycle arrest by carcinogen PAHs both in human and cells.

LncRNA *H19* has been closely related with human several diseases in recent studies (Chen et al., 2020; Wang et al., 2020), and its upregulated expression profile has been observed in a variety of human malignancies (Wang et al., 2019). Numerous studies found PAHs are known to trigger lung cancer in animals and humans (Petit et al., 2019). 1-OHP has been widely used as a biomarker of PAHs exposure and a urinary metabolite of pyrene in occupationally exposed population, which accounts for 1.2% - 13.4% of PAHs exposure in coke-oven plant (Olujimi et al., 2018). Additionally, *H19* binds to and inhibits SAHH function in vivo and vitro (Zhou et al., 2015; Oksana et al., 2013). In this cross-sectional study, a positive correlation was also observed between urinary 1-OHP levels and peripheral blood *H19* RNA expression in occupational workers, while a negative correlation between urinary 1-OHP levels and plasma SAHH activity was observed. Our previous vitro experiments exposed to BaP also yielded the consistent results (Fu et al., 2018).

One-carbon metabolism comprises complex biological networks in which input nutrients are processed through a series of chemical reactions to cycle carbon units. The produced metabolites are then made available for important processes including cellular biosynthesis, methylation, regulation of redox status and amino-acid homeostasis (Fedra et al., 2017). Essentially, one-carbon metabolism involves three pathways: the folate and methionine cycles, and the transsulfuration pathway. The folate and methionine cycles overlap upon the synthesis of methyltetrahydrofolate (MTHF) necessary for the generation of methionine through methylation of homocysteine (Tibbetts and Appling, 2010). Methionine is then converted into the fundamental metabolite SAM, the universal cellular methyl donor required for DNA, RNA, protein, and lipid methylation. SAHH is an enzyme, which catalyses the hydrolysis of SAH which is formed after the donation of the methyl group of SAM to a methyl acceptor in methylation reaction (Oksana et al., 2013; Li et al., 2013).Human SAHH forms a homotetramer consisting of 432 amino acid (aa) and is composed of four identical chemically identical and functionally equivalent subunits (Porcelli et al., 2000), each with three domains: a small C-terminal domain (386 - 432 aa), a cofactor-binding domain (197 - 351 aa) and a substrate-binding domain (1 - 181 aa and 355 - 385 aa) (Beluzić et al., 2008). Nonetheless, we know little about the amino acid residues involved in the catalytic mechanism of SAHH. And then, WT-SAHH (1 - 432 aa), M1-SAHH (1 - 150 aa), M2-SAHH (151 - 300 aa), M3-SAHH (300 - 432 aa) mutant versions of SAHH were constructed to explore association between amino acid sites of SAHH catalytic activity and the function of lncRNA *H19*. Whether exposed BaP or not, we observed an accessorial enrichment of *H19* in SAHH-containing RNPs in WT-SAHH, M1-SAHH and M2-SAHH cells, whereas M3-SAHH cells did not detectably elevate. Furthermore, *H19* RNA expressions were inhibited in *SAHH*-overexpressing cells compare to WT cells, particularly in M3-SAHH cells. Collectively, *H19* may bind to the 1 - 300 amino acid chain of SAHH to regulate oxidative DNA damage and cell cycle arrest exposed to BaP.

Otherwise, SAHH offers a single way in which catalyses the reversible SAH hydrolysis to relief from SAM-dependent methylation inhibition in eukaryotes (Oksana et al., 2013). Gene methylation, maintained strictly by the action of three DNMTs (DNMT1, DNMT3A and DNMT3B) in normal cells, is a key controller in a vast array of biological processes, such as DNA replication and repair (Oksana et al., 2004). Thus, the increase of SAHH activity would affect SAM-dependent DNMTs, which leads to the change of gene methylation. However, not all DNMTs are sensitive to SAHH. In one report, *H19*/SAHH/DNMT3B circuit regulates genome-wide methylation in human tumour cell models(Zhong et al., 2017), whereas Ponnaluri V.K. *et al* demonstrated that SAHH could enhance DNMT1 activity and interact with DNMT1 during S-phase in vitro (Ponnaluri et al., 2018). In this experiment, we found that whether treated cells with BaP or not, *H19* or SAHH single knockdown and *H19*/*SAHH* double knockdown attenuated DNMT3A (Fig. S1F) and DNMT3B protein expressions (Fig. S1G). However, *H19* or SAHH single knockdown and *H19*/*SAHH* double knockdown attenuated DNMT1 protein expressions and activity after BaP exposure. Moreover, the interaction of SAHH with DNMT1 would be strengthened by BaP and inhibition of *H19* enhanced the interaction of SAHH and DNMT1 induced by BaP. Furthermore, co-localization between endogenous *H19*, SAHH and DNMT1 was observed in nucleus and perinuclear cytoplasm. Our investigations revealed that *H19*/SAHH might regulate BaP-induced abnormal gene methylation via binding to DNMT1 and exaggerate its expression and activity.

PAHs have attracted much attention due to their carcinogenicity and its metabolism mechanisms occurred by cytochrome P450-mediated oxidase system may lead to oxidative DNA damage (Campo et al., 2020) and abnormal cell cycle distribution, especially S phase arrest (Andrysik et al., 2007). BaP, a potent carcinogenic PAHs, can cause cell cycle block, including elevated S-phase cells ratio, weakened DNA replication capacity, and inhibited cell proliferation (Hruba et al., 2010). Accordingly, we conducted the vitro experiment with BEAS-2B cells treated with BaP as a simulated condition and hope to provide insights into the epigenetic regulation mechanism of *H19*/SAHH/DNMT1. Moreover, 8-OHdG, a ROS-induced DNA base modification, is a sensitive and stable biomarker in the evaluation of DNA damage by oxidation factors (Davalli et al., 2018). Previous study also examined that a significantly elevated 8-OHdG levels (*OR* = 2.63, 95% *CI* = 1.04 - 6.66) and S phase arrest (*OR* = 2.76, 95% *CI* = 1.18 - 6.45) was associated with high levels of urinary 1-OHP in 385 study population (Fu et al., 2019). In this experiment, we have observed that suppression of *H19* reduced oxidative DNA damage and recovered S phase arrest, while suppression of SAHH and DNMT1 shows the opposite trend. It was validated that *H19* binding to SAHH interacts with DNMT1 to regulate oxidative DNA damage and cell cycle arrest in human lung epithelial cell lines after BaP exposure.

Further, BER is thought to be the vital guardian pathway participated in the removal of the common oxidative lesion 8-OHdG, which is initiated by OGG1 involving in the first step of this repair process (Castillejos et al., 2000). OGG1 is bifunctional enzyme: it is able to remove 8-OHdG paired with C and therefore distinguish between 8-OHdG and the vast majority of normal bases (Klungland and Bjelland, 2007). Previous studies have observed associations between PAHs exposure with global or gene-specific DNA methylation alterations (Herbstman et al., 2012). Both PAHs exposure and its related damages (e.g., oxidative stress) have been associated with DNA methylation alterations (Herbstman et al., 2012).

Moreover, exposure to some PAHs in $PM_{10}$ have reported to show a higher methylation level in specific DNA repair genes, such as *OGG1* and *APEX* (Alvarado-Cruz et al., 2016). Findings from the previous reports were consistent, which workers highly exposed to PAHs had an *OGG1* Pos.4 hypermethylation in comparison with the low-exposed employees (Hernandez-Cortes et al., 2018). Based on the aforementioned information, it led us to be curious about the role of *OGG1* methylation regulated by *H19*/SAHH/DMNT1 plays in oxidative DNA damage and cell cycle arrest related to BaP exposure. As expected, the significant rise occurred in *OGG1* methylation with BaP treatment, whereas the decrease was observed when *H19* was downregulated. Conversely, *SAHH* or *DNMT1* single knockdown exacerbated *OGG1* methylation. Interestingly, although *H19* single knockdown obviously reduced *OGG1* methylation, *H19*/*SAHH* and *H19*/*DNMT1* double knockdown abrogated this effect while *SAHH*/*DNMT1* double knockdown aggravated the alteration. It is further confirmed that *H19*/SAHH/DNMT1 can enhance the suppression of SAM-dependent biological methylation in BaP-treated cells, thereby reducing *OGG1* methylation. As stated above, oxidative DNA damage and S phase arrest was consistent to *OGG1* methylation. It also prompted that the alterations *OGG1* methylation may be related with oxidative DNA damage and S phase arrest in BaP-treated cells. These parallel results indicated that *H19*/SAHH/DNMT1 plays a critical role in oxidative DNA damage and cell cycle arrest by PAHs.

In summary, our results support the hypothesis that *H19*/SAHH/DNMT1 axis may be involved in *OGG1* methylation, oxidative DNA damage and cell cycle arrest by carcinogen BaP. The results in this study suggest the possible oxidative DNA damage and cell cycle arrest might reciprocally influence each other and form a vicious cycle, leading to greater severity DNA damage and even cancer. Further research should be aimed at a more detailed study of the specific mechanisms by which methylation occurs and plays a role in DNA damage.

Further, we have only studied oxidative DNA damage and cell cycle arrest in human lung epithelial cell lines, but have not shown any results on reactive oxygen species and χH2AX, which are the main markers of oxidative DNA damage. So, we will continue to have studied the effects of the parameters on ROS levels and expression of χH2AX in BEAS-2B cell line and lung cancer cell line, and published the research results in succession.

# Conclusions

Urinary 1-OHP, the vital urinary metabolite for PAHs exposure, was positively associated with peripheral blood *H19* RNA expression, while was negatively associated with plasma SAHH activity in occupational workers. BaP, the human carcinogen PAHs, contributed to the binding among *H19*, SAHH and DNMT1, which synergistically involved in regulating *OGG1* methylation, oxidative DNA damage and cell cycle arrest in human lung epithelial cell lines. Hence, we concluded from the study that *H19*/SAHH/DNMT1 plays an essential role in the *OGG1* methylation, oxidative DNA damage and cell cycle arrest.

# Abbreviations

1-OHP, 1-hydroxypyrene, 2-FLU, 2-hydroxyfluorene, 2-NAP, 2-hydroxynaphthalene, 9-PHE, 9-hydroxyphenanthrene, BaP, Benzo[*a*]pyrene, BER, Base excision repair, DNMT, DNA methyltransferase, lncRNAs, long noncoding RNAs, *OGG1*, Eight-oxoguanine DNA glycosylase 1, PAHs, Polycyclic aromatic hydrocarbons, ROS, reactive oxygen species, SAH, S-adenosylhomocysteine, SAHH, S-adenosylhomocysteine hydrolase, SAM, S-adenosylmethionine.

# Declarations

### Ethics approval and consent to participate

Our research was approved by the Ethical Review Board of the School of Public Health, Shanxi Medical University, Shanxi, People's Republic of China.

### Consent for publication

Not applicable.

### Availability of data and materials

Not applicable.

### Competing interests

The authors have no conflicts of interests to declare.


### Funding

This project was supported by the grants from National Nature Science Foundation of China [No. 81273041 and 30901180], Research Project Supported by Shanxi Scholarship Council of China [No. HGKY2019053] and Natural Science Foundation of Shanxi Province of China [No. 201701D121146].


### Authors' contributions

**Ye Fu:** Designed research, Performed research, Contributed new reagents or analytic tools, Analysed data, Wrote the paper. **Xuejing Li**: Designed research, Performed research, Analysed data, Wrote the paper. **Baolong Pan**: Performed research, Contributed new reagents or analytic tools, Wrote the paper. **Yingying Niu**: Performed research, Analysed data, Wrote the paper. **Bin Zhang:** Analysed data, Wrote the paper. **Xinyu Zhao**: Analysed data, Wrote the paper. **Jisheng Nie**: Project administration, Wrote the paper. **Jin Yang**: Funding acquisition, Project administration, Designed research, Performed research, Analysed data, Wrote the paper.


### Acknowledgements

We thank all researchers and study population from Steel Group General Hospital of Taiyuan.

# References


1. Alvarado-Cruz I, Sánchez-Guerra M, Hernández-Cadena L, et al. (2017) Increased methylation of repetitive elements and DNA repair genes is associated with higher DNA oxidation in children in an urbanized, industrial environment. *Mutation research* 813: 27-36.
2. Alvarado-Cruz I, Sánchez-Guerra M, Hernández-Cadena L, et al. (2016) Increased methylation of repetitive elements and DNA repair genes is associated with higher DNA oxidation in children in an urbanized, industrial environment. *Mutat Res* 813: 27-36.
3. Andres JL, Fan S, Turkel GJ, et al. (1998) Regulation of BRCA1 and BRCA2 expression in human breast cancer cells by DNA-damaging agents. *Oncogene* 16: 2229-2241.
4. Andrysik Z, Vondracek J, Machala M, et al. (2007) The aryl hydrocarbon receptor-dependent deregulation of cell cycle control induced by polycyclic aromatic hydrocarbons in rat liver epithelial cells. *Mutat Res* 615: 87-97.
5. Beluzić R, Cuk M, Pavkov T, et al. (2008) S-Adenosylhomocysteine hydrolase (AdoHcyase) deficiency: enzymatic capabilities of human AdoHcyase are highly effected by changes to codon 89 and its surrounding residues. *Biochem Biophys Res Commun* 368: 30-36.
6. Campo L, Hanchi M, Sucato S, et al. (2020) Biological Monitoring of Occupational Exposure to Metals in Electric Steel Foundry Workers and Its Contribution to 8-Oxo-7,8-Dihydro-2'-Deoxyguanosine Levels. *Int J Environ Res Public Health* 17.
7. Castillejos M, Borja-Aburto VH, Dockery DW, et al. (2000) Airborne Coarse Particles and Mortality. *Inhalation Toxicology* 12: 61-72.
8. Chen C, Liu M, Tang Y, et al. (2020) LncRNA H19 is involved in myocardial ischemic preconditioning via increasing the stability of nucleolin protein. *J Cell Physiol*.
9. Chen LL. (2016) Linking Long Noncoding RNA Localization and Function. *Trends Biochem Sci* 41: 761-772.
10. Davalli P, Marverti G, Lauriola A, et al. (2018) Targeting Oxidatively Induced DNA Damage Response in Cancer: Opportunities for Novel Cancer Therapies. *Oxidative medicine and cellular longevity* 2018: 2389523-2389523.
11. Fedra LM, Anna H-A, Noemi C, et al. (2017) Nutrients in Energy and One-Carbon Metabolism: Learning from Metformin Users. 9: 121.
12. Fu Y, Niu Y, Pan B, et al. (2019) OGG1 methylation mediated the effects of cell cycle and oxidative DNA damage related to PAHs exposure in Chinese coke oven workers. *Chemosphere* 224: 48-57.
13. Fu Y, Wang W, Li X, et al. (2018) LncRNA H19 interacts with S-adenosylhomocysteine hydrolase to regulate LINE-1 Methylation in human lung-derived cells exposed to Benzo[a]pyrene. *Chemosphere* 207: 84-90.
14. Gonçalves AC, Alves R, Baldeiras I, et al. (2017) Genetic variants involved in oxidative stress, base excision repair, DNA methylation, and folate metabolism pathways influence myeloid neoplasias susceptibility and prognosis. *Molecular Carcinogenesis* 56: 130-148.

15. Herbstman JB, Tang D, Zhu D, et al. (2012) Prenatal Exposure to Polycyclic Aromatic Hydrocarbons, Benzo[a]pyrene–DNA Adducts, and Genomic DNA Methylation in Cord Blood. *Environmental Health Perspectives* 120: 733-738.
16. Hernandez-Cortes D, Alvarado-Cruz I, SolãS-Heredia MJ, et al. (2018) Epigenetic modulation of Nrf2 and Ogg1 gene expression in testicular germ cells by methyl parathion exposure. *Toxicol Appl Pharmacol* 346: 19-27.
17. Hruba E, Trilecova L, Marvanova S, et al. (2010) Genotoxic polycyclic aromatic hydrocarbons fail to induce the p53-dependent DNA damage response, apoptosis or cell-cycle arrest in human prostate carcinoma LNCaP cells. *Toxicol Lett* 197: 227-235.
18. Idowu O, Semple KT, Ramadass K, et al. (2019) Beyond the obvious: Environmental health implications of polar polycyclic aromatic hydrocarbons. *Environ Int* 123: 543-557.
19. Illamola SM, Echaabi AK, Mazeron C, et al. (2019) Development and validation of a UPLC-UV method for the quantification of thiopurine methyltransferase enzyme activity in human erythrocytes. *J Chromatogr B Analyt Technol Biomed Life Sci* 1113: 91-97.
20. Kanduri C. (2015) Long noncoding RNAs: Lessons from genomic imprinting. *Biochimica Et Biophysica Acta* 1859: 102-111.
21. Klungland A and Bjelland S. (2007) Oxidative damage to purines in DNA: role of mammalian Ogg1. *DNA Repair (Amst)* 6: 481-488.
22. Li Q, Zhu L, Yan Y, et al. (2013) S-Adenosyl Homocysteine Hydrolase (SAHH) Accelerates Flagellar Regeneration in Dunaliella salina. 67: 249-254.
23. Moorthy B, Chu C and Carlin DJ. (2015) Polycyclic aromatic hydrocarbons: from metabolism to lung cancer. *Toxicol Sci* 145: 5-15.
24. Oksana T, Meinhard H and Kohlwein SD. (2004) S-adenosyl-L-homocysteine hydrolase in yeast: key enzyme of methylation metabolism and coordinated regulation with phospholipid synthesis. *Febs Letters* 577: 501-506.
25. Oksana T, Nermina M, Myriam V, et al. (2013) S-adenosyl-L-homocysteine hydrolase and methylation disorders: Yeast as a model system. 1832: 204-215.
26. Olujimi OO, Ogunseye OO, Oladiran KO, et al. (2018) Preliminary Investigation into Urinary 1-Hydroxypyrene as a Biomarker for Polycyclic Aromatic Hydrocarbons exposure among Charcoal Workers in Ogun and Oyo States, Nigeria. *Saf Health Work* 9: 416-420.
27. Petit P, Maitre A, Persoons R, et al. (2019) Lung cancer risk assessment for workers exposed to polycyclic aromatic hydrocarbons in various industries. *Environ Int* 124: 109-120.
28. Ponnaluri VKC, Esteve PO, Ruse CI, et al. (2018) S-adenosylhomocysteine Hydrolase Participates in DNA Methylation Inheritance. *J Mol Biol* 430: 2051-2065.
29. Porcelli M, Fusco S, Inizio T, et al. (2000) Expression, Purification, and Characterization of Recombinant S-Adenosylhomocysteine Hydrolase from the Thermophilic Archaeon Sulfolobus solfataricus. *Protein Expression & Purification* 18: 27-35.

30. Tibbetts AS and Appling DRJARoN. (2010) Compartmentalization of Mammalian folate-mediated one-carbon metabolism. 30: 57-81.
31. Wang J, Sun J and Yang F. (2020) The role of long non-coding RNA H19 in breast cancer. *Oncol Lett* 19: 7-16.
32. Wang J, Xie S, Yang J, et al. (2019) The long noncoding RNA H19 promotes tamoxifen resistance in breast cancer via autophagy. *J Hematol Oncol* 12: 81.
33. Whitaker AM, Schaich MA, Smith MR, et al. (2017) Base excision repair of oxidative DNA damage: from mechanism to disease. *Front Biosci (Landmark Ed)* 22: 1493-1522.
34. Yang J, Liu X, Niu P, et al. (2009) Correlations and co-localizations of Hsp70 with XPA, XPG in human bronchial epithelia cells exposed to benzo[a]pyrene. 265: 10-14.
35. Yang J, Zhang H, Zhang H, et al. (2017) Smoking modify the effects of polycyclic aromatic hydrocarbons exposure on oxidative damage to DNA in coke oven workers. *International Archives of Occupational & Environmental Health* 90: 1-9.
36. Zhong T, Men Y, Lu L, et al. (2017) Metformin alters DNA methylation genome-wide via the H19/SAHH axis. *Oncogene* 36: 2345-2354.
37. Zhou J, Yang L, Zhong T, et al. (2015) H19 lncRNA alters DNA methylation genome wide by regulating S-adenosylhomocysteine hydrolase. *Nat Commun* 6: 10221-10233.

# Tables

**Table 1.** Basic characteristics of participants by urinary 1-OHP among 146 occupational workers [a]

| Variable | Urinary 1-OHP (μg/mmol creatinine) | | | | | *P* value [b] |
|---|---|---|---|---|---|---|
| | Total (n = 146) | Quartile 1 (< 0.03) (n = 36) | Quartile 2 (0.03 - 0.06) (n = 36) | Quartile 3 (0.06 - 0.11) (n = 37) | Quartile 4 (> 0.11) (n = 37) | |
| **General characteristic** | | | | | | |
| Age (years) | 40.5 (10) | 39.5 (9) | 44.0 (11) | 43.0 (10) | 39.0 (12) | 0.144 |
| Employment time (years) | 21.0 (12) | 20.0 (12) | 26.5 (13) | 24.0 (10) | 19.0 (17) | 0.053 |
| Smoking | 105 (71.9) | 26 (72.2) | 27 (75.0) | 27 (73.0) | 25 (67.6) | 0.910 |
| Drinking | 73 (50.0) | 18 (50.0) | 15 (41.7) | 20 (54.1) | 20 (54.1) | 0.685 |
| Central heating | 140 (95.9) | 33 (91.7) | 36 (100.0) | 35 (94.6) | 36 (97.3) | 0.319 |
| Education (years) | | | | | | 0.367 |
| ≤ 9 | 41 (28.1) | 10 (27.8) | 13 (36.1) | 6 (16.2) | 12 (32.4) | |
| 10 - 12 | 57 (39.0) | 12 (33.3) | 14 (38.9) | 15 (40.5) | 16 (43.2) | |
| > 12 | 48 (32.9) | 14 (38.9) | 9 (25.0) | 16 (43.2) | 9 (24.3) | |
| **PAHs internal exposure biomarker** | | | | | | |
| 2-NAP | 0.74 (0.77) | 0.62 (0.71) | 0.70 (0.50) | 0.53 (0.58) | 1.13 (1.43) | 0.001 |
| 2-FLU | 0.29 (0.27) | 0.18 (0.13) | 0.27 (0.17) | 0.25 (0.29) | 0.53 (0.63) | < 0.001 |
| 9-PHE | 0.09 (0.09) | 0.06 (0.03) | 0.07 (0.04) | 0.09 (0.07) | 0.23 (0.22) | < 0.001 |
| ΣOH-PAHs | 0.32 (0.29) | 0.23 (0.18) | 0.27 (0.20) | 0.32 (0.20) | 0.51 (0.56) | < 0.001 |

Concentration unit of 2-NAP, 2-FLU, 9-PHE and 1-OHP is μg/mmol creatinine.

[a] Data were presented as *N* (%) or Med (IQR).

[b] *P*-values were calculated from Chi-square test for categorical variables and Kruskal-Wallis H test for numerical variables.

# Figures

### Figure 1

Associations between urinary 1-OHP and peripheral blood H19 RNA expression, plasma SAHH activity (n = 146) (a) A violin plot showed the distributions of peripheral blood H19 RNA expression and plasma SAHH activity. P-values of the numerical variable were calculated by Mann-Whitney U test. The red line represents mean, the blue line represents median, the blue indicates the range from 25th percentile to 75th percentile, and the wathet blue indicates the range from 5th percentile to 95th percentile. (b) Effects of urinary 1-OHP on peripheral blood H19 RNA expression and plasma SAHH activity. Q = quartile. Data were presented as odds ratio (OR) and 95% confidence interval (95% CI). Model 1: adjusted for employment time, education, age, drinking status, smoking status and heating mode. Model 2: additional adjusted for urinary 2-FLU, 2-NAP, 9-PHE. The median of blood H19 RNA Expression as cut point: < 14.42 (0), ≥ 14.42 (1). The median of plasma SAHH Activity as cut point: < 0.83 (0), ≥ 0.83 (1). (c) Restricted cubic spline model for peripheral blood H19 RNA expression and plasma SAHH activity across urinary 1-OHP levels. Adjusted for employment time, education, age, drinking status, smoking status, heating mode, 2-FLU, 2-NAP and 9-PHE. The median of peripheral blood H19 RNA Expression as cut point: < 14.42 (0), ≥ 14.42 (1). The median of plasma SAHH Activity as cut point: < 0.83 (0), ≥ 0.83 (1).

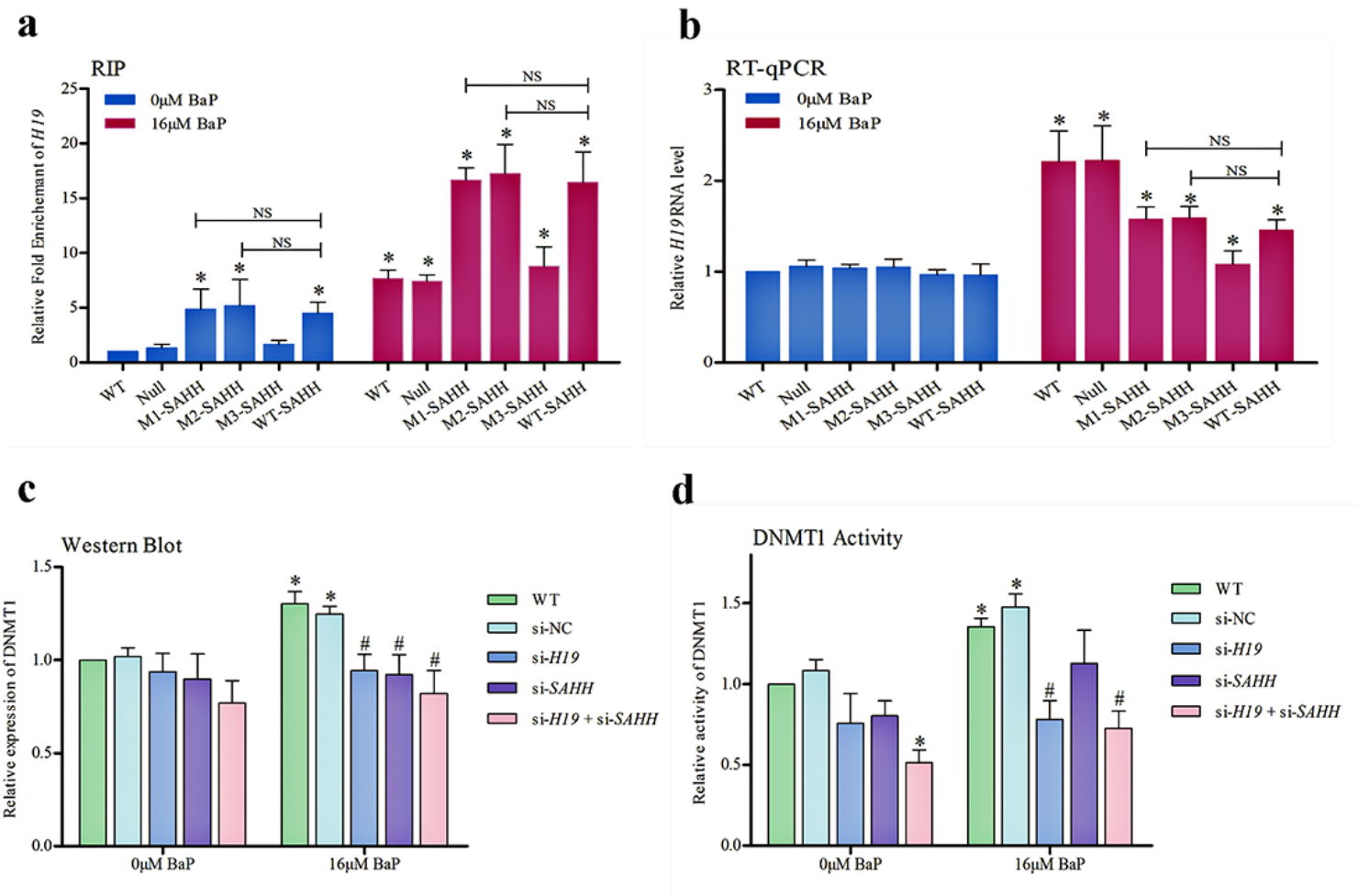


## Figure 2

H19 interacts with SAHH at specific sites and then regulates DNMT1 in BEAS-2B cells exposed to BaP (a) RIP analysis was performed to test the interaction between SAHH protein and H19 mRNA. The relative fold enrichment of H19 in SAHH-containing RNPs without BaP treatment were set as 1. The results were representative of three independent experiments with similar results (n=6). *P < 0.05: compared with the relative fold enrichment of H19 in SAHH-containing RNPs exposed to no BaP for 24 h. NS: P > 0.05. (b) After transfection, RT-PCR was performed to detect H19 RNA levels. The results were representative of three independent experiments with similar results (n=9). *P < 0.05: compared with WT cells exposed to no BaP for 24 h. NS: P > 0.05. (c) Western blot was performed to detect DNMT1 protein expression. The numbers at the bottom of the blots show DNMT1 protein expressions by using β-Tubulin as an invariant internal control. The results were representative of three independent experiments with similar results (n=9). *P < 0.05: compared with WT cells exposed to no BaP for 24 h. (d) DNMT1 activity levels in five types of BEAS-2B (WT, si-NC, si-H19, si-SAHH, si-H19 + si-SAHH) exposed to no or 16 μM BaP for 24 hours. *P < 0.05 vs. WT cells treated with 0μM BaP for 24 hours. # P < 0.05 vs. WT cells treated with 16 μM BaP for 24 hours. NS: not significant.

## Figure 3

H19 binding to SAHH interacts with DNMT1 in BEAS-2B cells exposed to BaP (a) Co-immunoprecipitation was performed to measure the binding of endogenous SAHH and DNMT1. Levels of Co-IP-purified SAHH were determined with western blot and presented as fold enrichment in anti-DNMT1 relative to Input SAHH. Relative fold enrichment of SAHH in DNMT1-containing proteins without BaP treatment were set as 1. The results were representative of three independent experiments with similar results (n=5). IgG was used as a control. *P < 0.05 vs. WT cells treated with 0μM BaP for 24 hours. (b) Co-localization studies between endogenous H19, SAHH and DNMT1. Representative images showed the localization of H19 (red), SAHH (green) and DNMT1 (blue). DAPI (sky blue) was using to stain Nuclei. Orange spots represent the colocalization between H19 and SAHH. Purple spots represent the colocalization between H19 and DNMT1. Aquamarine blue spots represent the colocalization between SAHH and DNMT1. Blue violet spots represent the colocalization between endogenous H19, SAHH and DNMT1.

**Figure 4**

H19/SAHH/DNMT1 regulates OGG1 methylation to affect oxidative DNA damage and cell cycle arrest (a) The schematic diagram shows that there are four CpG loci in the first exon of OGG1 which we selected. Heat map represents the coefficient of (r) of the Spearman correlation between the mean of four CpG loci and each locus in OGG1. (b) H19/SAHH/DNMT1 regulates OGG1 methylation in cells treated with BaP. Relative OGG1 methylation was presented with that in WT cells without BaP exposure arbitrarily set as 1. The results were representative of three independent experiments with similar results (n=6). *P < 0.05: compared with WT cells exposed to no BaP for 24 h. (c) H19/SAHH/DNMT1 affects oxidative DNA damage in cells treated with BaP. Relative 8-OHdG levels was presented with that in WT cells without BaP exposure arbitrarily set as 1. The results were representative of three independent experiments with similar results (n=9). *P < 0.05: compared with WT cells exposed to no BaP for 24 h. (d) H19/SAHH/DNMT1 affects cell cycle in cells treated with BaP. Relative cell cycle ratio (S phase) was presented with that in WT cells without BaP exposure arbitrarily set as 1. The results were representative of three independent experiments with similar results (n=10). *P < 0.05: compared with W T cells exposed to no BaP for 24 h.

# Supplementary Files

This is a list of supplementary files associated with this preprint. Click to download.

- FigS1.tif
- SupplementaryInformation.docx